Journal of Sound and Vibration (1999) **220**(1), 155–170
Article No. jsvi.1998.1956, available online at http://www.idealibrary.com on IDEAL

BIFURCATION AND RESONANCE OF A MATHEMATICAL MODEL FOR NON-LINEAR MOTION OF A FLOODED SHIP IN WAVES

S. MURASHIGE AND K. AIHARA

Department of Mathematical Engineering and Information Physics, Graduate School of Engineering, The University of Tokyo, Japan

AND

M. KOMURO

Department of Electronics and Information Science, Teikyo University of Science and Technology, Japan

(*Received* 27 *April* 1998, *in final form* 1 *September* 1998)

A flooded ship can exhibit undesirable non-linear roll motion even in waves of moderate amplitude. In order to understand the mechanism of this non-linear phenomenon, the non-linearly coupled dynamics of a ship and flood water are considered using a mathematical model for the simplified motion of a flooded ship in regular beam waves. This paper describes bifurcation and resonance of this coupled system. A bifurcation diagram shows that large-amplitude subharmonic motion exists in a wide range of parameters, and that the Hopf bifurcation is observed due to the dynamic effects of flood water. Resonance frequencies can be determined by linearization of this model. Comparison between the resonance points and the bifurcation curves suggests that non-linear resonances of this model can bring about large-amplitude subharmonic motion, even if it is in the non-resonant state of the linearized system.

1. INTRODUCTION

The non-linear motion of a ship in waves may lead to a serious accident such as capsizing. For example, in 1994 the ferry *Estonia* capsized quickly after a large amount of sea water flooded into the vehicle-deck with a wide open area reserved for the transportation of vehicles. Although the possibility of the vehicle-deck flooding was recognised, existing safety standards, based mainly on static stability, were met. Following this accident, experimental investigations suggested that the ship's non-linear response to waves, including complicated bifurcation phenomena, may have indeed been related to the sinking of the *Estonia* [1, 2]. For this reason, the authors feel that dynamic stability should be studied further to avoid such disasters in the future.

0022–460X/99/060155 + 16 $30.00/0

Non-linear ship motion in waves has been considered from the viewpoint of non-linear dynamics using a mathematical model for roll motion of a ship in waves [3–9]. Virgin [3] claimed that prediction of chaotic roll motion may be a useful indicator of imminent capsizing. Nayfeh *et al*. [7] and Thompson and de Souza [8] examined non-linear coupling of roll and the other modes. Falzarno *et al*. [9] studied static effects of flood water on roll motion in waves. Our previous experimental work [1] demonstrated that the non-linearly coupled dynamics of the ship and flood water was the key to understanding the complicated non-linear response of a flooded ship in waves. After this experimental determination, a mathematical model was derived for the coupled motion in waves [2].

The main objectives of the present paper are to analyse the bifurcations of the non-linearly coupled system of roll and flood water using the mathematical model derived in reference [2], and to examine the mechanism of the complicated non-linear response. Section 2 describes modelling of this coupled motion and summarizes some characteristics of the model. Section 3 shows numerical examples of bifurcation sets. This model can be regarded as a coupled oscillatory system which has three representative frequencies, namely a wave frequency, a natural frequency of roll motion of a ship, and a natural frequency of oscillatory motion of flood water. From these, resonance frequencies of the system can be determined. Section 4 discusses the relation between the bifurcation phenomena and non-linear resonances.

2. A MATHEMATICAL MODEL FOR MOTION OF A FLOODED SHIP IN WAVES

2.1. MODELLING OF COUPLED MOTION OF ROLL AND FLOOD WATER IN WAVES

Previous experimental work [1] demonstrated that the coupled motion of roll and flooded water was dominant in this problem. The simplified motion of a flooded box-shaped ship in a vertical cross-section in the direction of progress of waves is considered, as shown in Figure 1, assuming that: (a) coupling of roll

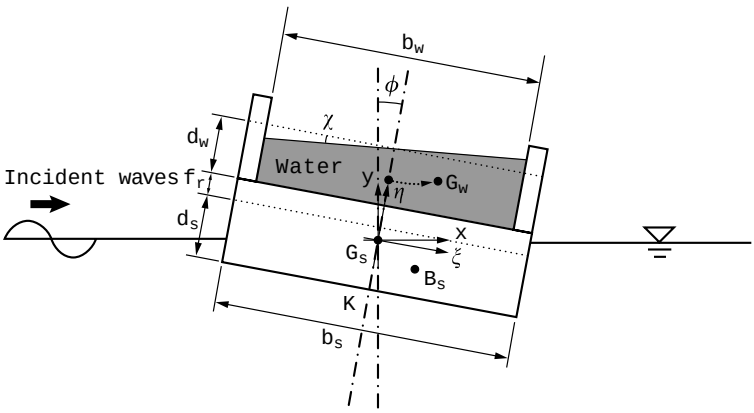

Figure 1. Illustration of the simplified motion of a flooded ship in waves. ϕ: roll angle of a ship, χ: slope of the surface of flood water, b_s: breadth of a ship, b_w: breadth of an inside area of a ship, d_s: draft, f_r: freeboard, d_w: depth of flood water, G_s: center of gravity of a ship, G_w: center of gravity of flood water, and B_s: center of buoyancy of a ship.

motion and flood water is dominant, and sway and heave modes can be neglected; (b) the surface of the flood water is flat with the slope χ; (c) the motion of the flood water can be approximated by that of a material particle located at the center of gravity G_w; (d) the wave forcing moment varies sinusoidally with the same angular frequency Ω as the incident waves; and (e) the damping moments on the ship and flood water vary linearly with $\dot{\phi}$ and $\dot{\chi}$ ($\dot{} = \mathrm{d}/\mathrm{d}t$), respectively. In Figure 1, x and y denote the horizontal and vertical co-ordinates, respectively, with the origin set at the center of gravity of the ship G_s.

Based on the above assumptions, the kinetic energy K, the potential energy P, and the rate of energy dissipation D can be expressed as

$$\begin{aligned}
K_s &= \tfrac{1}{2}(I + \delta I)\dot{\phi}^2 = \tfrac{1}{2}M\kappa^2\dot{\phi}^2,\\
K_w &= \tfrac{1}{2}m(\dot{x}_{G_w}^2 + \dot{y}_{G_w}^2),\\
P_s &= -\rho V g y_{B_s} = -(M+m)g y_{B_s},\\
P_w &= m g y_{G_w},\\
P_f &= -\phi\{A_0 + A_1 \sin(\Omega t + \psi)\},\\
D &= \tfrac{1}{2}v_s\dot{\phi}^2 + \tfrac{1}{2}v_w\dot{\chi}^2,
\end{aligned} \tag{1}$$

where the subscripts s, w, and f denote the ship, the flood water, and the wave forcing moment, I and δI the moment and the added moment of inertia about the axis of roll, M and m the masses of the ship and of the flood water, κ the radius of gyration, g the gravitational acceleration, $\mathbf{x}_{G_w} = (x_{G_w}, y_{G_w})$ the location of the center of gravity of the flood water G_w, $\mathbf{x}_{B_s} = (x_{B_s}, y_{B_s})$ the location of the center of buoyancy B_s of the ship, $A_0 + A_1 \sin(\Omega t + \psi)$ the wave forcing moment, and v the damping coefficient, respectively. We can obtain a mathematical model for the coupled motion by substituting K, P, and D into Lagrange's equations of motion as follows:

$$\frac{\mathrm{d}}{\mathrm{d}t}\left(\frac{\partial L}{\partial \dot{\phi}}\right) - \frac{\partial L}{\partial \phi} + \frac{\partial D}{\partial \dot{\phi}} = 0, \qquad \frac{\mathrm{d}}{\mathrm{d}t}\left(\frac{\partial L}{\partial \dot{\chi}}\right) - \frac{\partial L}{\partial \chi} + \frac{\partial D}{\partial \dot{\chi}} = 0, \tag{2}$$

where the Lagrangian $L = K - P$, $K = K_s + K_w$, and $P = P_s + P_w + P_f$. For the sake of convenience, $\mathbf{x}_{B_s}$ and $\mathbf{x}_{G_w}$ are expressed as

$$\mathbf{x}_{B_s} = \begin{pmatrix} x_B(\phi) \\ y_B(\phi) \end{pmatrix},$$

$$\mathbf{x}_{G_w} = \begin{pmatrix} x_G(\phi, \chi) \\ y_G(\phi, \chi) \end{pmatrix}$$

$$= \begin{pmatrix} \cos\phi, & \sin\phi \\ -\sin\phi, & \cos\phi \end{pmatrix}\begin{pmatrix} \xi_G(\chi) \\ \eta_G(\chi) \end{pmatrix}, \tag{3}$$

and the kinetic energy of flood water K_w as

$$K_w = \tfrac{1}{2}m(q_1(\chi)\dot{\phi}^2 + 2q_2(\chi)\dot{\phi}\dot{\chi} + q_3(\chi)\dot{\chi}^2), \tag{4}$$

where

$$\begin{aligned} q_1(\chi) &= \xi_G^2 + \eta_G^2, \\ q_2(\chi) &= \frac{\partial \xi_G}{\partial \chi} \cdot \eta_G - \xi_G \cdot \frac{\partial \eta_G}{\partial \chi}, \\ q_3(\chi) &= \left(\frac{\partial \xi_G}{\partial \chi}\right)^2 + \left(\frac{\partial \eta_G}{\partial \chi}\right)^2. \end{aligned} \tag{5}$$

Normalizing each mass and length by M and κ, respectively, one can write the equations of motion in the form

$$\mathbf{M}\ddot{\boldsymbol{\theta}} + \mathbf{N}\dot{\boldsymbol{\theta}} + \mathbf{h} + \mathbf{r} = \mathbf{f}, \tag{6}$$

with

$$\boldsymbol{\theta} = (\phi, \chi)^T,$$

$$\mathbf{M} = \begin{pmatrix} 1 + \rho\tilde{q}_1, & \rho\tilde{q}_2 \\ \rho\tilde{q}_2, & \rho\tilde{q}_3 \end{pmatrix},$$

$$\mathbf{N} = \begin{pmatrix} \tilde{v}_s, & 0 \\ 0, & \tilde{v}_w \end{pmatrix},$$

$$\mathbf{h} = \begin{pmatrix} \rho\left(\dfrac{\partial \tilde{q}_1}{\partial \chi}\dot{\phi}\dot{\chi} + \dfrac{\partial \tilde{q}_2}{\partial \chi}\dot{\chi}^2\right) \\ \tfrac{1}{2}\rho\left(-\dfrac{\partial \tilde{q}_1}{\partial \chi}\dot{\phi}^2 + \dfrac{\partial \tilde{q}_3}{\partial \chi}\dot{\chi}^2\right) \end{pmatrix},$$

$$\mathbf{r} = (r_1, r_2)^T,$$

$$\begin{cases} r_1 = -(1+\rho)\sigma^2 \dfrac{\partial \tilde{y}_B}{\partial \phi} - \rho\sigma^2(\tilde{\xi}_G \cos\phi + \tilde{\eta}_G \sin\phi), \\ r_2 = \rho\sigma^2\left(-\dfrac{\partial \tilde{\xi}_G}{\partial \chi}\sin\phi + \dfrac{\partial \tilde{\eta}_G}{\partial \chi}\cos\phi\right), \end{cases}$$

$$\mathbf{f} = \begin{pmatrix} \tilde{A}_0 + \tilde{A}_1 \sin(\Omega t + \psi) \\ 0 \end{pmatrix}, \tag{7}$$

where T denotes the transpose, $\rho = m/M$, $\sigma = \sqrt{g/\kappa}$, $\tilde{q}_{1,2,3} = q_{1,2,3}/\kappa^2$, $\tilde{\xi}_G = \xi_G/\kappa$, $\tilde{\eta}_G = \eta_G/\kappa$, $\tilde{v}_{s,w} = v_{s,w}/(M\kappa^2)$, and $\tilde{A}_{0,1} = A_{0,1}/(M\kappa^2)$, respectively. Hereafter this form

is used with the tilde omitted. Note that the time t is not normalized. Equation (6) can be rewritten in the form

$$\frac{\mathrm{d}\mathbf{u}}{\mathrm{d}t} = \mathbf{F}(t, \mathbf{u}), \tag{8}$$

where $\mathbf{u} = (\phi, \chi, \dot{\phi}, \dot{\chi})^T$ and

$$\mathbf{F} = \begin{pmatrix} \dot{\boldsymbol{\theta}} \\ \mathbf{M}^{-1}(-\mathbf{N}\dot{\boldsymbol{\theta}} - \mathbf{h} - \mathbf{r} + \mathbf{f}) \end{pmatrix}. \tag{9}$$

2.2. SOME CHARACTERISTICS OF THE MATHEMATICAL MODEL

Based on the above assumptions, $\mathbf{x}_{B_s}$ corresponds to the center of the cross-section of the ship under the still water surface, and, similarly, $\mathbf{x}_{G_w}$ the center of the cross-section of flood water. Each sectional shape changes from a trapezoid to a triangle at $\phi = \phi^* = \tan^{-1} 2d_s/b_s$ and $\chi = \chi^* = \tan^{-1} 2d_w/b_w$, respectively, as shown in Figure 2. The co-ordinates $y_B(\phi)$, $\xi_G(\chi)$, and $\eta_G(\chi)$ in equation (7) are shown in Appendix A. Then, the vector $\mathbf{F}$ in equation (8) is continuous with respect to ϕ and χ, but the Jacobian matrix $\partial\mathbf{F}/\partial\mathbf{u}$ is discontinuous at $\phi = \phi^*$ and $\chi = \chi^*$.

The forcing term is expressed as the sum of the constant heel moment A_0 and the periodically fluctuating one $A_1 \sin(\Omega t + \psi)$. Only when $A_0 = 0$, this model has a symmetrical property as follows:

$$\mathbf{F}\left(t + \frac{\pi}{\Omega}, \boldsymbol{\Lambda}\mathbf{u}\right) = \boldsymbol{\Lambda}\mathbf{F}(t, \mathbf{u}) \qquad \text{when } A_0 = 0, \tag{10}$$

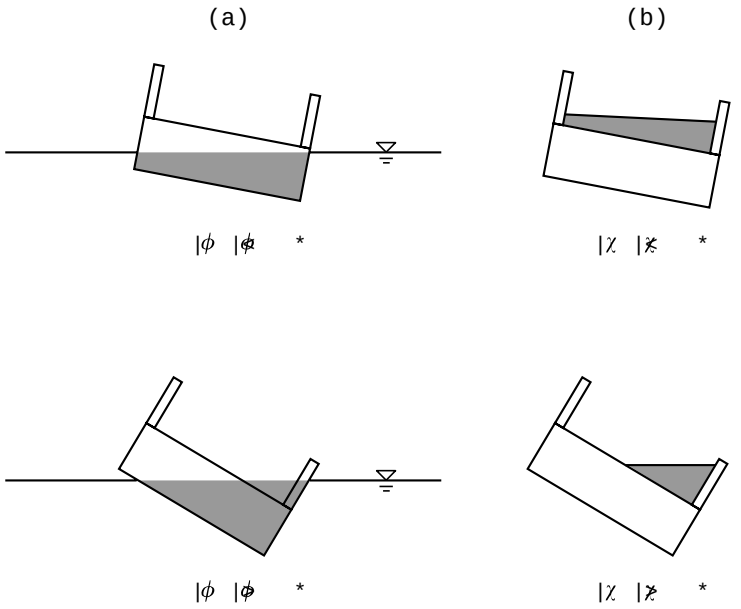

Figure 2. Variation of sectional shapes with ϕ and χ. Shaded regions show the cross-sections of (a) the ship under the still water level and (b) flood water. $\phi^* = \tan^{-1} 2d_s/b_s$; $\chi^* = \tan^{-1} 2d_w/b_w$.

where

$$\mathbf{\Lambda} = \begin{pmatrix} -1 & 0 & 0 & 0 \\ 0 & -1 & 0 & 0 \\ 0 & 0 & -1 & 0 \\ 0 & 0 & 0 & -1 \end{pmatrix}. \tag{11}$$

In real phenomena, A_0 (>0) is much smaller than A_1.

3. BIFURCATION ANALYSIS

This section shows some numerical examples of bifurcation of the mathematical model equation (6) under almost the same conditions as the experiment using a ferry model [1]. Each parameter is set as follows: $\rho = m/M = 0{\cdot}19$, $b_s = 2{\cdot}689$, $b_w = 1{\cdot}936$, $d_s = 0{\cdot}874$, $d_w = 0{\cdot}194$, $d_s + f_r = 0{\cdot}958$. $\overline{KG_s} = 0{\cdot}915$, $v_s = 0{\cdot}03$, $v_w = 0{\cdot}024$, and $\psi = 0{\cdot}0$. Figure 3 displays phase portraits of two different periodic solutions, one with the period $2\pi/\Omega$ (“period 1”) and another one $4\pi/\Omega$ (“period 2”), for $\Omega = 2\pi/6{\cdot}98$, $A_0 = 0{\cdot}0$, and $A_1 = 0{\cdot}02$. It can be seen that large-amplitude subharmonic motion “period 2” coexists with small-amplitude harmonic motion “period 1”. This result agrees with the experimental results [1].

Next, in order to examine stability of the “period-N” solutions, the Poincaré map $\mathbf{T}$ is defined by

$$\mathbf{T}: \mathbf{u}_0 \mapsto \mathbf{T}(\mathbf{u}_0) = \boldsymbol{\varphi}\left(t = t_0 + N\frac{2\pi}{\Omega}, \mathbf{u}_0\right), \tag{12}$$

where $\boldsymbol{\varphi}(t, \mathbf{u}_0)$ denotes a solution of equation (8) with the initial values $\mathbf{u}(t = t_0) = \mathbf{u}_0$. The “period-$N$” solutions satisfy the fixed point condition

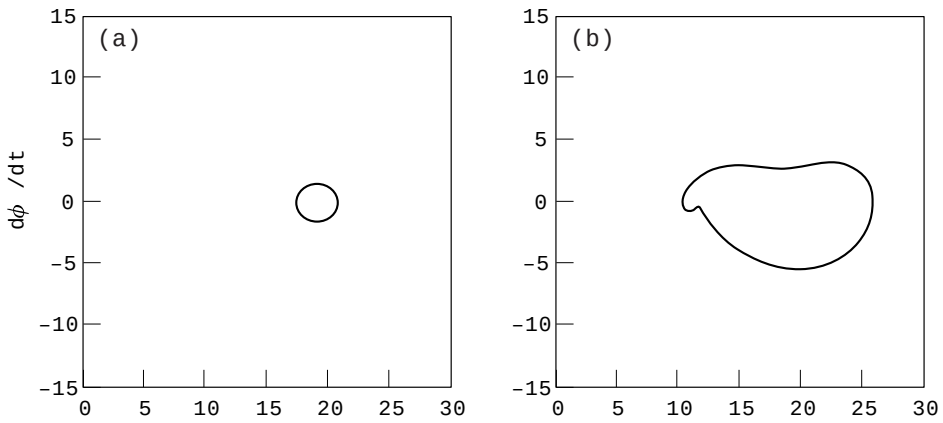

Figure 3. Phase portraits of two different periodic solutions in $(\phi, \dot{\phi})$. $\Omega = 2\pi/6{\cdot}98$; $A_0 = 0{\cdot}0$; $A_1 = 0{\cdot}02$. (a) Period 1; (b) period 2.

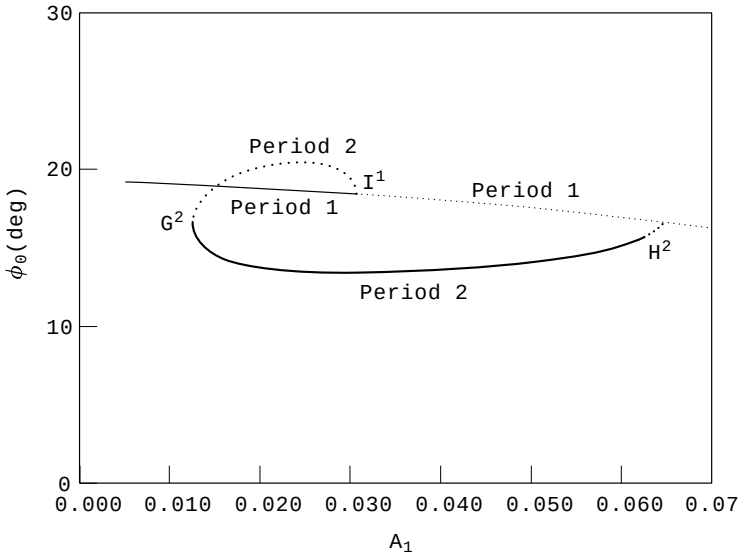

Figure 4. Variation of the roll angle ϕ_0 at the fixed point of the two periodic solutions, "period 1" and "period 2" solutions in Figure 3, with changing A_1. $\phi_0 = \phi(t_0) = \phi(t_0 + (2\pi/\Omega))$ for the "period 1" solutions, and $\phi_0 = \phi(t_0) = \phi(t_0 + 2 \times (2\pi/\Omega))$ for the "period 2" solutions at the same phase of the forcing term **f** in equation (6), namely $\Omega t_0 + \psi = 0$. Solid line: stable ($|\mu|_{max} < 1$); dotted line: unstable ($|\mu|_{max} > 1$); μ: eigenvalue, I^N: period doubling bifurcation; G^N: saddle-node bifurcation; H^N: Hopf bifurcation; N: "period N".

$\mathbf{u}_0 = \mathbf{T}(\mathbf{u}_0)$. One can trace the fixed points with changing parameters, examine the stability, and determine the bifurcation points of the "period-N" solutions by numerically computing eigenvalues μ_i ($i = 1 \sim 4$) of $\partial\mathbf{T}/\partial\mathbf{u}_0$ [10]. Note that stability analysis requires careful treatment of the non-smoothness of this system shown in section 2.2 [11]. Figure 4 shows the variation of the roll angle ϕ at the fixed point of the two periodic solutions in Figure 3 with changing A_1. In this figure, the axis of ordinate ϕ_0 denotes the roll angle ϕ at the fixed point of the same phase of the forcing term **f** in equation (6), such that $\phi_0 = \phi(t_0) = \phi(t_0 + (2\pi/\Omega))$ for the "period 1" solutions, and $\phi_0 = \phi(t_0) = \phi(t_0 + 2 \times (2\pi/\Omega))$ for the "period 2" solutions. Note that only one point, namely ϕ only at $t = t_0$, is plotted for both periodic solutions. Solid and dotted lines represent the stable and unstable periodic solutions, respectively. It is found that these two periodic solutions coexist for $0{\cdot}0126 < A_1 < 0{\cdot}0624$. This is because at the subcritical period-doubling bifurcation point I_1 of the "period 1" solution, the unstable "period 2" solution is generated, and at the saddle-node bifurcation point G_2, the unstable "period 2" solution disappears by coalescence with the stable "period 2" solution. This bifurcation structure enables small-amplitude "period 1" and large-amplitude "period 2" solutions to coexist, as shown in Figure 3. Furthermore, the stable "period 2" solution bifurcates to quasi-periodic motion at H^2.

Figure 5 shows a bifurcation diagram of "period 1" and "period 2" solutions in the parameter space (Ω, A_1). One can see that stable subharmonic motion "period 2" exists for a wide range of parameters. In addition, note that the Hopf bifurcation is observed in this diagram. This result characterizes non-linearly

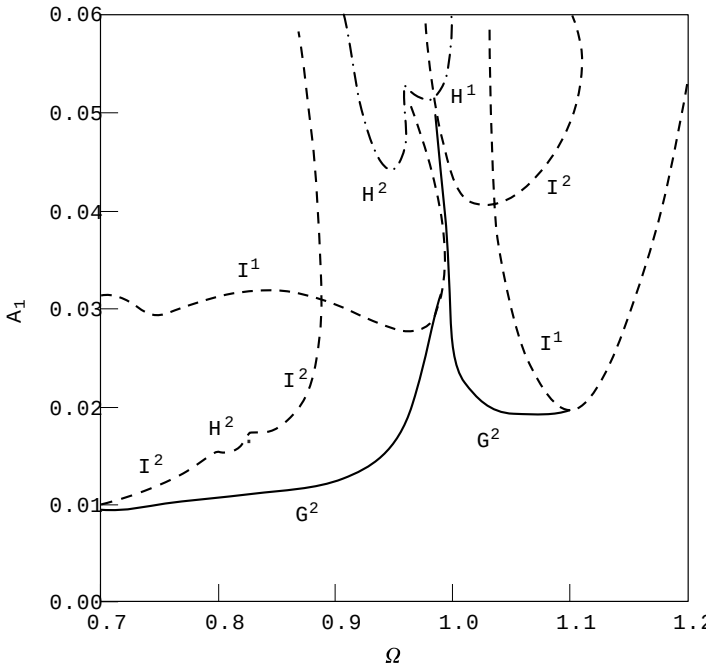

Figure 5. Bifurcation diagram in the (Ω, A_1)-plane. The wave frequency Ω (rad/s) is represented in a real time scale. Solid line (G^N): Saddle-node bifurcation. Dashed line (I^N): period doubling bifurcation; dot-dashed line (H^N): Hopf bifurcation; N: "period N".

coupled dynamics because, when a ship has no flood water, or when dynamic effects of flood water are neglected, the Hopf bifurcation cannot occur in this model, similarly to Duffing's equation [10].

4. RESONANCE OF THE NON-LINEARLY COUPLED SYSTEM OF A SHIP AND FLOOD WATER IN WAVES

This mathematical model is a coupled oscillatory system subjected to a periodic forcing. Thus it may be natural to consider that non-linear resonances of this system are related to bifurcation phenomena. In order to discuss this point, resonance frequencies are obtained by linearizing this model, and compared with bifurcation points of "period 1" solutions in Figure 5.

When a ship is flooded in still water, namely $\rho > 0$, it has two statistically balanced positions at $\phi = \pm\phi_e$ ($\phi_e > 0$). Here the only case considered is when the ship is initially set at $\phi = \phi_e$. When the wave amplitude is small, the ship rolls around this equilibrium position with small amplitude. Then ϕ and χ can be expressed as

$$\begin{aligned}\phi(t) &= \phi_e + \phi_1(t),\\ \chi(t) &= \chi_e + \chi_1(t)\\ &= \phi + \chi_1(t)\\ &= \phi_e + \phi_1(t) + \chi_1(t).\end{aligned} \tag{13}$$

Here it should be noted that the equilibrium angle of χ is not ϕ_e but ϕ. In order to linearize the model, assume the order of ϕ_1, χ_1, v_s, v_w, A_0, and A_1 as follows:

$$\begin{aligned} \phi_1 &= O(\varepsilon), \qquad \chi_1 = O(\varepsilon), \\ v_s &= O(\varepsilon), \qquad v_w = O(\varepsilon), \\ A_0 &= O(\varepsilon^2), \qquad A_1 = O(\varepsilon), \end{aligned} \tag{14}$$

where $\varepsilon \ll 1$. Each term in equation (6) is expanded and arranged as follows:

$$\begin{aligned} q_i &= q_{i0} + O(\varepsilon), \qquad \text{for } i = 1, 2, 3, \\ -\frac{\partial y_B}{\partial \phi} &= \alpha_0 + \alpha_1 \phi_1 + O(\varepsilon^2), \\ \xi_G &= \beta_0 + \beta_1(\phi_1 + \chi_1) + O(\varepsilon^2), \\ \eta_G &= \gamma_0 + \gamma_1(\phi_1 + \chi_1) + O(\varepsilon^2), \\ \frac{\partial \xi_G}{\partial \chi} &= \beta_0' + \beta_1'(\phi_1 + \chi_1) + O(\varepsilon^2), \\ \frac{\partial \eta_G}{\partial \chi} &= \gamma_0' + \gamma_1'(\phi_1 + \chi_1) + O(\varepsilon^2), \end{aligned} \tag{15}$$

where coefficients α_j, β_j, γ_j, β_j', and γ_j' $(j = 0, 1)$ are shown in Appendix B. Then the 0th and the 1st order equations can be written as follows:

0th order equation: $O(\varepsilon^0)$

$$(1 + \rho)\alpha_0 - \rho(\beta_0 C_e + \gamma_0 S_e) = 0. \tag{16}$$

1st order equations: $O(\varepsilon^1)$

$$\mathbf{M}_1 \ddot{\boldsymbol{\theta}}_1 + \mathbf{R}_1 \boldsymbol{\theta}_1 = \mathbf{f}_1, \tag{17}$$

with

$$\boldsymbol{\theta}_1 = (\phi_1, \chi_1)^T,$$

$$\mathbf{M}_1 = \begin{pmatrix} m_{11}, & m_{12} \\ m_{21}, & m_{22} \end{pmatrix},$$

$$\begin{cases} m_{11} = 1 + \rho(q_1 + q_2), \\ m_{12} = \rho q_2, \\ m_{21} = \rho(q_2 + q_3), \\ m_{22} = \rho q_3, \end{cases}$$

$$\mathbf{R}_1 = \begin{pmatrix} r_{11}, & r_{12} \\ r_{21}, & r_{22} \end{pmatrix},$$

$$\begin{cases} r_{11} = (1+\rho)\sigma^2\alpha_1 - \rho\sigma^2\{(-\beta_0+\gamma_1)S_e + (\gamma_0+\beta_1)C_e\}, \\ r_{12} = -\rho\sigma^2(\beta_1 C_e + \gamma_1 S_e), \\ r_{21} = 0, \\ r_{22} = -r_{12}, \end{cases}$$

$$\mathbf{f}_1 = \begin{pmatrix} A_1 \sin(\Omega t + \psi) \\ 0 \end{pmatrix}, \tag{18}$$

where $S_e = \sin\phi_e$ and $C_e = \cos\phi_e$. The equilibrium angle ϕ_e is determined by the 0th order equation (15). Natural frequencies ω_1 and ω_2 of the 1st order equations (16) are given by

$$\omega_{1,2} = (s \pm \sqrt{s^2 - |\mathbf{M}_1||\mathbf{R}_1|})/|\mathbf{M}_1|, \tag{19}$$

with $2s = m_{11}r_{22} + m_{22}r_{11} - m_{12}r_{21} - m_{21}r_{12}$. Figures 6 and 7 show variation of the equilibrium angle ϕ_e and the natural frequencies ω_1 and ω_2 with the amount of flood water, respectively, for the same parameter values as in section 3. In the 1st order system, resonances occur only at $\Omega = \omega_1$ and $\Omega = \omega_2$. For higher order systems, it should be noticed that non-linear terms in the model include trigonometric functions which produce non-linearities to any order. Thus, this model can exhibit subharmonic resonances at $\Omega = 2\omega_{1,2}, 3\omega_{1,2}, \ldots$, superharmonic

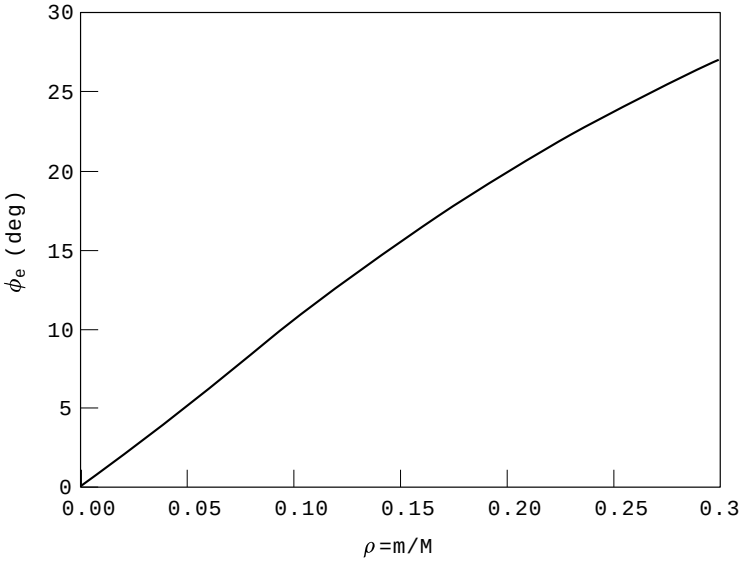

Figure 6. Variation of the equilibrium angle ϕ_e with the ratio of the amount of flooded water to the displacement of a ship $\rho = m/M$. The parameter values are the same as those in section 3.

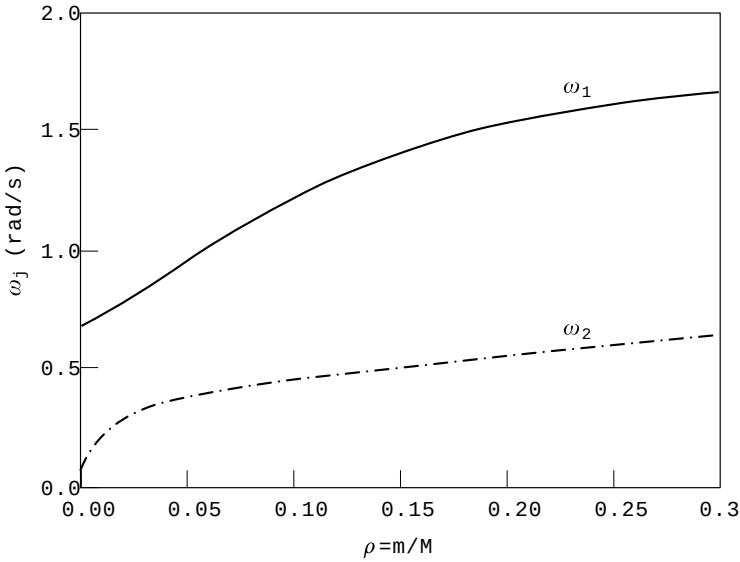

Figure 7. Variation of natural frequencies ω_1 and ω_2 with the ratio of the amount of flood water to the displacement of a ship $\rho = m/M$. The parameter values are the same as those in section 3.

resonances at $\Omega = \omega_{1,2}/2, \omega_{1,2}/3, \ldots$, and combination resonances $\Omega = n_1\omega_1 \pm n_2\omega_2$ ($n_{1,2} = 1, 2, \ldots$) [12]. In the case of the numerical example in section 3, $\omega_1 = 1{\cdot}518$ and $\omega_2 = 0{\cdot}550$.

Figure 8 shows frequency response curves of the amplitude of (a) roll motion and (b) oscillatory motion of flood water of "period 1" solutions in Figure 5. The four curves in this figure display different frequency responses for $A_1 = 0{\cdot}002$, $0{\cdot}005$, $0{\cdot}010$, and $0{\cdot}022$. It is found that the amplitude of periodic motions becomes large at some resonance frequencies which are indicated by the dot-dashed line. This figure also shows that, when A_1 is small, primary resonances occur only at $\Omega = \omega_1$ and $\Omega = \omega_2$, and that, with an increase in A_1, higher order resonances become evident. Figure 9 shows the variation of the maximum absolute value of the eigenvalue $|\mu|_{max}$ with the wave frequency Ω for (a) $A_1 = 0{\cdot}002$ and (b) $A_1 = 0{\cdot}022$, respectively. Solutions are stable for $|\mu|_{max} < 1$ and unstable for $|\mu|_{max} > 1$. Similarly to Figure 8, some resonance frequencies are shown by the dot-dashed lines. In Figure 5, the period-doubling bifurcation of "period 1", I^1, is observed in two regions, one for $\Omega < 1{\cdot}0$ and another one for $\Omega > 1{\cdot}02$. The minimum points of the amplitude A_1 of these two bifurcation curves are located at $\Omega \sim \omega_1 - \omega_2 = 0{\cdot}968$ and $\Omega \sim 2\omega_2 = 1{\cdot}100$. Figure 9(b) shows that the "period 1" solutions become unstable near these two resonance frequencies. These results indicate that higher order resonances of this coupled system are deeply related to the complicated bifurcation structure found in Figure 5. Furthermore, comparison between Figures 5, 8 and 9 suggests that large-amplitude "period 2" solutions exist in the non-resonant state of the linearized system. Thus, these non-linear resonances should be taken into consideration in ship design, since the existing design rule requires stability only in the primarily resonant state in which the natural frequency of roll motion of a ship is close to the wave frequency Ω.

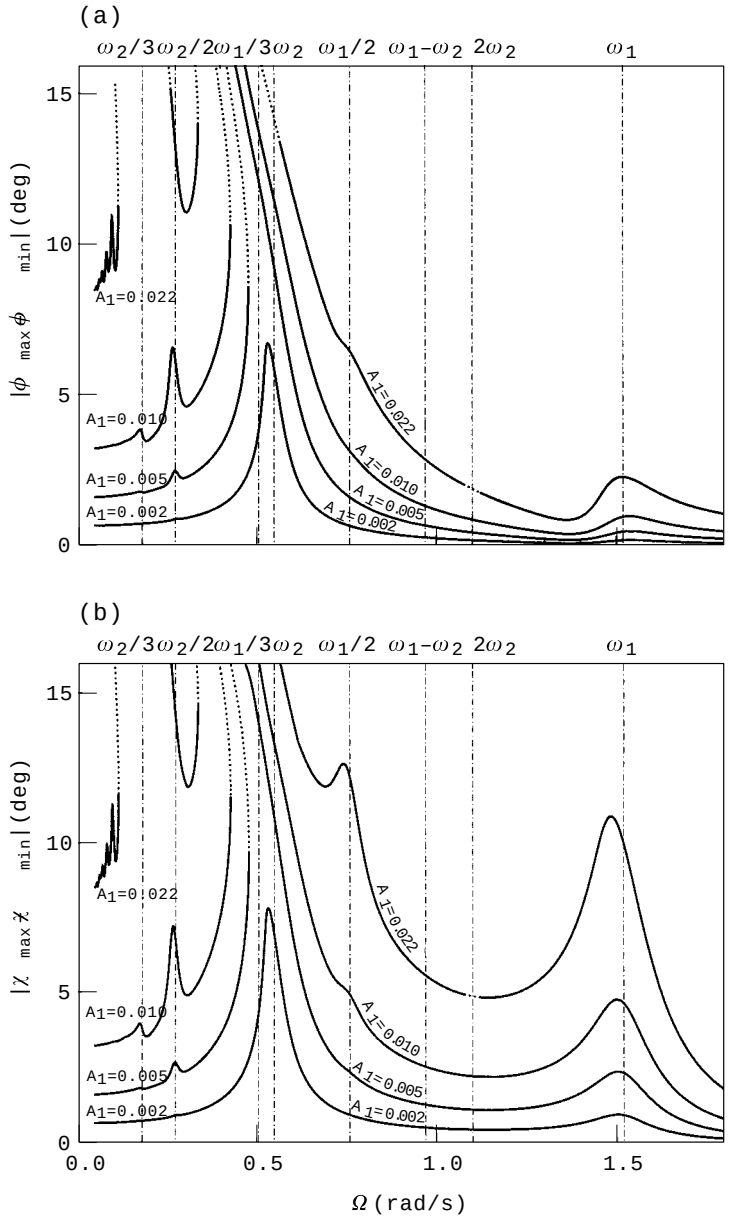

Figure 8. Frequency response curves of amplitude of (a) roll motion and (b) oscillatory motion of flood water of "period 1" solutions in Figure 5. ϕ: the roll angle, χ: the slope of flood water. Solid line: stable; dotted line: unstable; dot-dashed line: resonance frequencies. The frequency range is wider than that in Figure 5.

It is well known that internal resonances occur at $\omega_1 = n\omega_2$ $(n = 1, 2, \ldots)$ [8, 12]. Thompson and de Souza [8] pointed out that this resonance can suppress destabilization of ship motion. In the above numerical example, ω_1 is close to $3\omega_2$. This point will be studied elsewhere. In addition, although resonance frequencies can be estimated by the linearized system, further bifurcation analyses are required

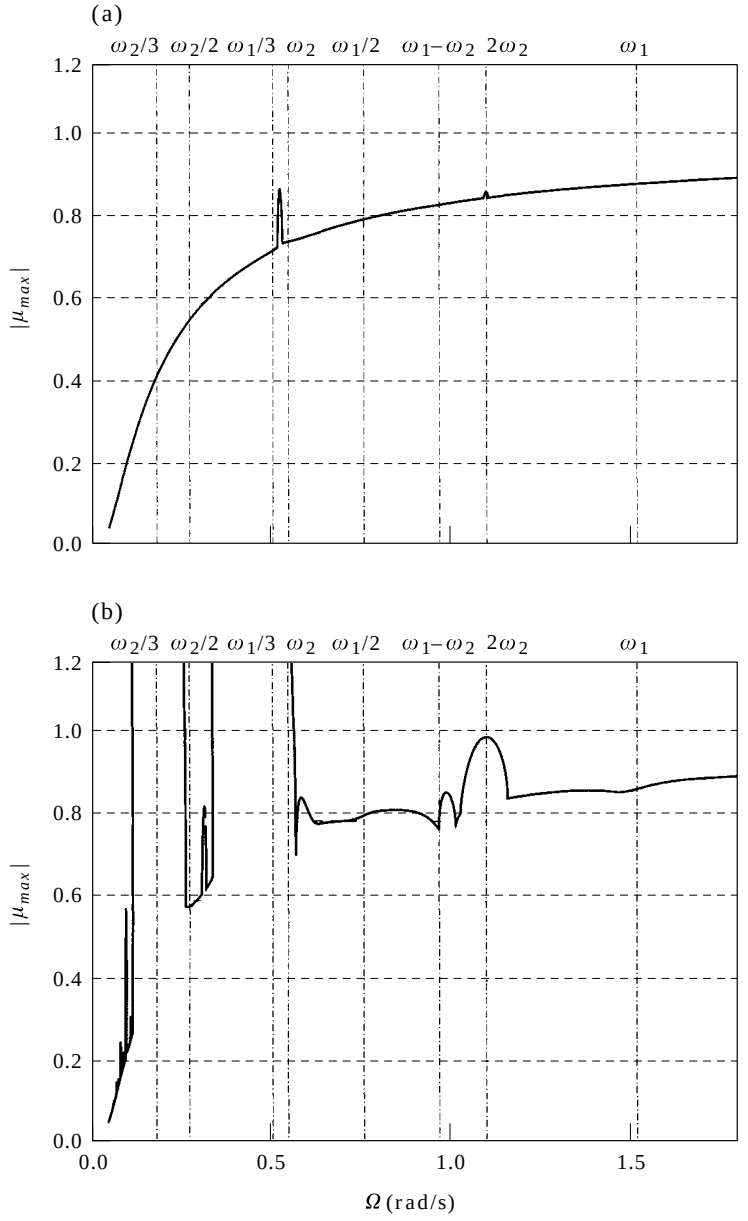

Figure 9. Variation of the maximum absolute value of the eigenvalue $|\mu|_{max}$ of "period 1" solutions in Figure 5 with changing Ω. Dot-dashed line: resonance frequencies. The frequency range is wider than that in Figure 5. (a) $A_1 = 0{\cdot}002$; (b) $A_1 = 0{\cdot}022$.

for fully understanding the complex mechanisms of non-linear phenomena, including chaos found in experiments.

5. CONCLUSIONS

On the basis of previous experimental work, a mathematical model for the motion of a flooded ship in waves has been analysed. This model is a coupled

oscillatory system of a ship and flood water subjected to wave forcing. Thus, this coupled oscillatory model has three representative frequencies, namely the wave frequency, the natural frequency of the roll motion of the ship, and the natural frequency of the oscillatory motion of the flood water. These frequencies and resonance frequencies were identified by linearizing the model equations.

Bifurcation analyses of periodic solutions of this model demonstrate that large-amplitude subharmonic motion exists for a wide range of wave frequencies and amplitudes, and that this system can exhibit a Hopf bifurcation due to the dynamic effects of flood water. Comparison between the bifurcation curves and the resonance points shows that higher order resonances of this coupled system can give rise to complicated bifurcation phenomena, even if it is in the non-resonant state of the linear system.

ACKNOWLEDGMENTS

The authors thank Professor Hiroshi Kawakami, Dr Tetsuya Yoshinaga, and Dr Tetsushi Ueta of Tokushima University for their helpful discussions. This work was supported by Special Coordination Funds for Promoting Science and Technology (SCF).

REFERENCES

1. S. Murashige and K. Aihara *Proceedings of Royal Society of London A* (to be published). Experimental study on chaotic motion of a flooded ship in waves.
2. S. Murashige and K. Aihara 1998 *International Journal of Bifurcation and Chaos* **8**, 619–626. Coexistence of periodic roll motion and chaotic one in a forced flooded ship.
3. L. N. Virgin 1987 *Applied Ocean Research* **9**, 89–95. The nonlinear rolling response of a vessel including chaotic motions leading to capsize in regular seas.
4. M. S. Soliman and J. M. T. Thompson 1991 *Applied Ocean Research* **13**, 82–92. Transient and steady state analysis of capsize phenomena.
5. H. Kan and H. Taguchi 1994 *Nonlinearity and Chaos in Engineering Dynamics* (J. M. T. Thompson and S. R. Bishop, editors), 418–420. Chichester: Wiley. Ship capsizing and chaos.
6. J. M. T. Thompson 1997 *Applied Mechanics Review* **50**, 307–325. Designing against capsize in beam seas: recent advances and new insights.
7. A. H. Nayfeh, D. T. Mook and L. R. Marshall 1973 *Journal of Hydronautics* **7**, 145–152. Nonlinear coupling of pitch and roll modes in ship motions.
8. J. M. T. Thompson and J. R. de Souza 1996 *Proceedings of Royal Society of London A* **452**, 2527–2550. Suppression of escape by resonant modal interactions: in shell vibration and heave-roll capsize.
9. J. M. Falzarno, S. W. Shaw and A. W. Troesch 1992 *International Journal of Bifurcation and Chaos* **2**, 101–115. Application of global methods for analyzing dynamical systems to ship rolling motion and capsizing.
10. H. Kawakami 1984 *IEEE Transactions on Circuits and Systems* CAS-**31**, 248–260. Bifurcation of periodic responses in forced dynamic nonlinear circuits: computation of bifurcation values of the system parameters.
11. S. Murashige, M. Komuro and K. Aihara 1997 *Proceedings of* 1997 *International Symposium on Nonlinear Theory and its Applications* (*NOLTA* '97) **1**, 497–500. Non-smooth characteristics and bifurcation of a mathematical model for motion of a flooded ship in waves.
12. A. H. Nayfeh and D. T. Mook 1979 *Nonlinear Oscillations*. New York: Wiley.

APPENDIX A: LOCATIONS OF THE CENTER OF BUOYANCY OF A SHIP AND THE CENTER OF GRAVITY OF FLOOD WATER

The co-ordinates y_B, ξ_G, and η_G in equation (7) are shown as follows:

Case 1. *Sectional shapes are trapezoidal* ($|\phi| < \phi^*, |\chi| < \chi^*$)

$$\begin{aligned} y_B &= l_1 C_\phi - \tfrac{1}{2} l_2 T_\phi S_\phi, \\ \xi_G &= l_3 T_\chi, \\ \eta_G &= \tfrac{1}{2} l_3 T_\chi^2 + l_4 + l_5. \end{aligned} \tag{A1}$$

Case 2. *Sectional shapes are triangular* ($|\phi| \geqslant \phi^*, |\chi| \geqslant \chi^*$)

$$\begin{aligned} y_B &= -\operatorname{sgn}(\phi) \cdot l_6 S_\phi + l_7 \sqrt{S_{2|\phi|}} - l_8 C_\phi, \\ \xi_G &= \operatorname{sgn}(\chi) \cdot \left(l_9 - l_{10} \frac{C_\chi}{\sqrt{S_{2|\chi|}}} \right), \\ \eta_G &= \operatorname{sgn}(\chi) \cdot l_{10} \frac{S_\chi}{\sqrt{S_{2|\chi|}}} + l_4, \end{aligned} \tag{A2}$$

where $l_1 = (d_s/2 - \overline{KG_s})/\kappa$, $l_2 = \overline{B_s M_s}/\kappa = b_s^2/(12 d_s \kappa)$, $l_3 = \overline{G_w M_w}/\kappa = b_w^2/(12 d_w \kappa)$, $l_4 = (d_s + f_r - \overline{KG_s})/\kappa$, $l_5 = d_w/(2\kappa)$, $l_6 = b_s/(2\kappa)$, $l_7 = (2/3)\sqrt{b_s d_s}/\kappa$, $l_8 = \overline{KG_s}/\kappa$, $l_9 = b_w/(2\kappa)$, $l_{10} = (2/3)\sqrt{b_w d_w}/\kappa$, $S_\phi = \sin\phi$, $C_\phi = \cos\phi$, $T_\phi = \tan\phi$, $S_{2|\phi|} = \sin 2|\phi|$, $S_\chi = \sin\chi$, $C_\chi = \cos\chi$, $T_\chi = \tan\chi$, $S_{2|\chi|} = \sin 2|\chi|$, $\tan\phi^* = 2d_s/b_s$, and $\tan\chi^* = 2d_w/b_w$, respectively.

APPENDIX B: COEFFICIENTS IN EQUATION (14)

Since small amplitude motion around the equilibrium point $\phi = \phi_e$ (>0) in the linearized system is considered, coefficients in equation (14) for $\phi > 0$ and $\chi > 0$ are shown as follows.

Case 1. *Sectional shapes are trapezoidal* ($0 < \phi < \phi^*, 0 < \chi < \chi^*$)

$$\begin{aligned} q_{10} &= (l_4 + l_5)^2 + (l_3 + l_4 + l_5) l_3 T_e^2 + \tfrac{1}{4} l_3^2 T_e^4, \\ q_{20} &= l_3 (1 + T_e^2)(l_4 + l_5 - \tfrac{1}{2} l_{10} T_e^2), \\ q_{30} &= l_3 (1 + T_e^2)^3, \\ \alpha_0 &= \{ l_1 + \tfrac{1}{2} l_2 (2 + T_e^2) \} S_e, \\ \alpha_1 &= \{ l_1 + \tfrac{1}{2} l_2 (2 + T_e^2) \} C_e + l_2 T_e (1 + T_e^2) S_e, \\ \beta_0 &= l_3 T_e, \qquad \beta_1 = l_3 (1 + T_e^2), \\ \beta_0' &= l_3 (1 + T_e^2), \qquad \beta_1' = 2 l_3 T_e (1 + T_e^2), \\ \gamma_0 &= l_4 + l_5 + \tfrac{1}{2} l_3 T_e^2, \qquad \gamma_1 = l_3 T_e (1 + T_e^2), \\ \gamma_0' &= l_3 T_e (1 + T_e^2), \qquad \gamma_1' = l_3 T_e (1 + T_e^2)(1 + 3 T_e^2). \end{aligned} \tag{B1}$$

Case 2. *Sectional shapes are triangular* ($\phi \geqslant \phi^*, \chi \geqslant \chi^*$)

$$q_{10} = l_4^2 + l_9^2 + l_{10}^2 \frac{1}{S_{2e}} + 2l_{10}\left(\frac{-l_9 C_e + l_4 S_e}{\sqrt{S_{2e}}}\right),$$

$$q_{20} = l_{10}\left(\frac{l_4 C_e - l_9 S_e + l_{10}\sqrt{S_{2e}}}{S_{2e}^{3/2}}\right),$$

$$q_{30} = l_{10}^2 \frac{1}{S_{2e}^3},$$

$$\alpha_0 = l_6 C_e - l_8 S_e - l_7 \frac{C_{2e}}{\sqrt{S_{2e}}},$$

$$\alpha_1 = -l_6 S_e - l_8 C_e + l_7\left(\frac{1 + S_{2e}^2}{S_{2e}^{3/2}}\right),$$

$$\beta_0 = l_9 - l_{10}\frac{C_e}{\sqrt{S_{2e}}}, \qquad \beta_1 = l_{10}\frac{1}{2S_e\sqrt{S_{2e}}},$$

$$\beta_0' = l_{10}\frac{C_e}{S_{2e}^{3/2}}, \qquad \beta_1' = l_{10}\frac{C_e}{S_{2e}^{3/2}}\left(\frac{T_e^2 - 3}{2T_e}\right),$$

$$\gamma_0 = l_4 + l_{10}\frac{S_e}{\sqrt{S_{2e}}}, \qquad \gamma_1 = l_{10}\frac{1}{2C_e\sqrt{S_{2e}}},$$

$$\gamma_0' = l_{10}\frac{S_e}{S_{2e}^{3/2}}, \qquad \gamma_1' = l_{10}\frac{S_e}{S_{2e}^{3/2}}\left(\frac{3T_e^2 - 1}{2T_e}\right), \tag{B2}$$

where $S_e = \sin\phi_e$, $C_e = \cos\phi_e$, $T_e = \tan\phi_e$, $S_{2e} = \sin 2\phi_e$, and $C_{2e} = \cos 2\phi_e$.